Journal of Medicinal Chemistry

ARTICLE

pubs.acs.org/jmc

Discovery of a Tetrahydroisoquinoline-Based Hydroxamic Acid Derivative (ZYJ-34c) as Histone Deacetylase Inhibitor with Potent Oral Antitumor Activities

Yingjie Zhang,[†] Hao Fang,[†] Jinhong Feng,[†] Yuping Jia,[†] Xuejian Wang,[†] and Wenfang Xu*[,†]

[†]Department of Medicinal Chemistry, School of Pharmacy, Shandong University, Ji'nan, Shandong, 250012, P.R. China

Supporting Information

ABSTRACT:

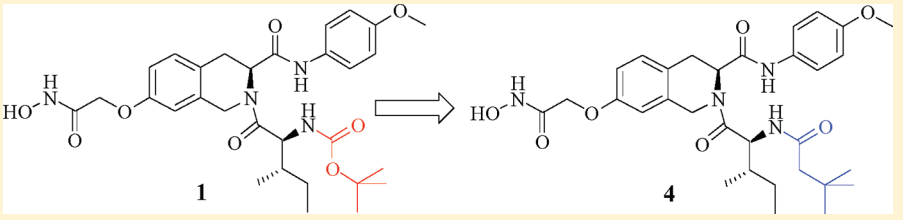

Histone deacetylase (HDAC) has emerged as an attractive target for the development of antitumor agents during the past decade. Previously tetrahydroisoquinoline-bearing hydroxamic acid analogue, ZYJ-25e (**1**), was identified and validated as a potent histone deacetylase inhibitor (HDACi) with marked in vitro and in vivo antitumor potency. In the present study, further modification of **1** led to another more potent, orally active HDACi, ZYJ-34c (**4**). Compared to FDA-approved drug suberoylanilide hydroxamic acid (SAHA), compound **4** exhibited higher in vivo antitumor potency in a human breast carcinoma (MDA-MB-231) xenograft model and in a mouse hepatoma-22 (H22) pulmonary metastasis model and similar in vivo antitumor potency in a human colon tumor (HCT116) xenograft model.

INTRODUCTION

HDACs are amidohydrolases which play multiple roles in the epigenetic regulation of gene expression, the remodeling of chromatin, and other crucial biological functions. The enzyme functions by removing the acetyl moiety from the ε—amino group of lysine residues of nucleosomal histone and various other nonhistone protein substrates.[1,2]

Eighteen HDACs, grouped into four classes, have been identified in humans. The enzymes of classes I (HDACs 1—3 and 8), II (HDACs 4—7, 9 and 10), and IV (HDACs 11) are all metalloproteases. It has been suggested that Zn^{2+}-dependent HDACs, especially class I and class II isozymes, are involved in tumorigenesis and development, and HDACs inhibition could cause proliferation inhibition, apoptosis, cellular differentiation, susceptibility to chemotherapy, antiangiogenesis, and migration inhibition of tumor cells.[3] Therefore, numerous structurally diverse HDACs inhibitors (HDACi) against Zn^{2+}-dependent HDACs have been developed.[4,5] Indeed, over 10 HDACi are currently in clinical trials as antitumor agents,[5] and two of them, SAHA (Figure 1)[6] and FK228 (Figure 1),[7] are already on the market. The class III HDACs (sirtuins 1—7) are NAD^+ dependent and are not yet strongly implicated in tumor.[8,9]

All Zn^{2+}-dependent HDACs share many common features in their highly conserved active site including a long, narrow hydrophobic tunnel leading to a cavity that contains a catalytic Zn^{2+} ion. Inhibitors of these HDACs also have a common general pharmacophore consisting of three domains: a zinc-binding group (ZBG) that coordinates to the catalytic Zn^{2+} in the active site, a cap group that interacts with the residues at the rim of active site entrance, and a linker that occupies the active site tunnel and tethers ZBG to cap (Figure 1).

On the basis of the HDACi pharmacophore, in our previous study we designed and synthesized a novel series of tetrahydroisoquinoline-bearing hydroxamic acid derivatives as HDACi (Figure 1).[10,11] Through several rounds of structural optimization, compound *tert*-butyl (2*S*,3*S*)-1-((*S*)-7-(2-(hydroxyamino)-2-oxoethoxy)-3-(4-methoxyphenylcarbamoyl)-3,4-dihydroisoquinolin-2(1*H*)-yl)-3-methyl-1-oxopentan-2-ylcarbamate, ZYJ-25e (**1**)[11] (Figure 2) was found to have promising in vitro and in vivo antitumor potency. In the follow-up structure modification, the substitution of tertiary amine group for amide group of **1** led to compounds *tert*-butyl (2*S*,3*S*)-1-((*S*)-7-(2-(hydroxyamino)-2-oxoethoxy)-3-(4-methoxyphenylcarbamoyl)-3,4-dihydroisoquinolin-2(1*H*)-yl)-3-methylpentan-2-ylcarbamate, ZYJ-34a (**2**)[11] and (*S*)-2-((2*S*,3*S*)-2-(3,3-dimethylbutanamido)-3-methylpentyl)-7-(2-(hydroxyamino)-2-oxoethoxy)-*N*-(4-methoxyphenyl)-1,2,3,4-tetrahydroisoquinoline-3-carboxamide, ZYJ-34b (**3**)[11] (Figure 2), both of which showed better water solubility in the salt form. Compound **2** exhibited more potent in vivo

Received: May 8, 2011
Published: June 29, 2011

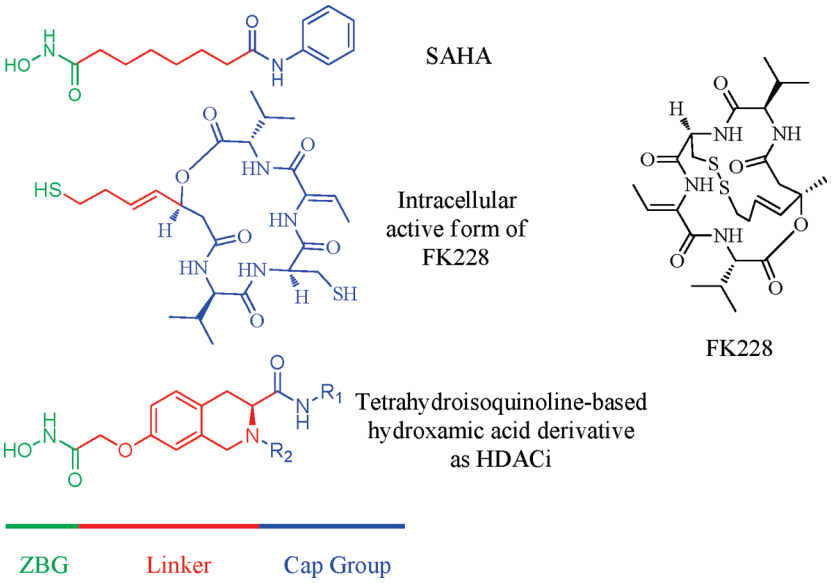

Figure 1. HDACi pharmacophore model and structures of SAHA, FK228, and our tetrahydroisoquinoline-based hydroxamic acid derivative.

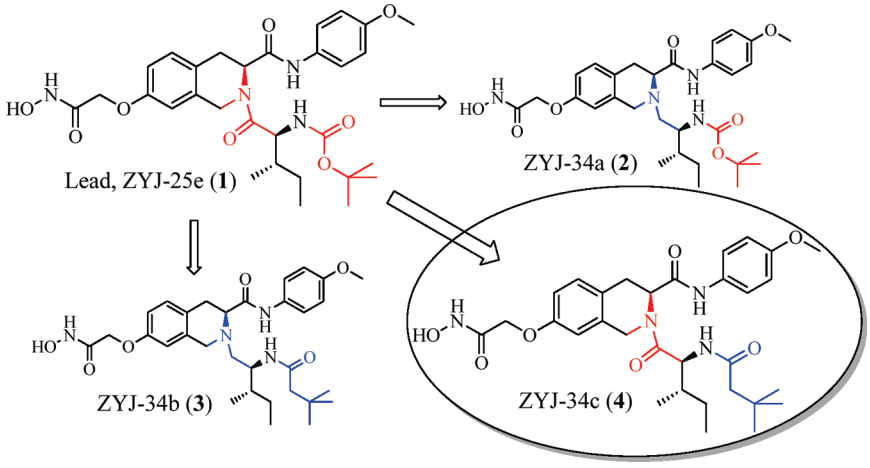

Figure 2. Structure comparison of **4** with its parent compound **1** and its analogues **2**, **3**.

antitumor activity than **1** and SAHA in a MDA-MB-231 xenograft model.[11] In the present study, considering that the gastric acid sensitive tertiary butyloxycarbonyl (Boc) group of **1** might be destroyed through oral administration and that the carbamate of **1** might be unstable against metabolism,[12,13] compound (*S*)-2-((2*S*,3*S*)-2-(3,3-dimethylbutanamido)-3-methylpentanoyl)-7-(2-(hydroxyamino)-2-oxoethoxy)-*N*-(4-methoxyphenyl)-1,2,3,4-tetrahydroisoquinoline-3-carboxamide, ZYJ-34c (**4**), was designed (Figure 2). Different from compounds **2** and **3**, compound **4** was derivatized from **1** with the amide group unchanged because the in vitro structure−activity relationship (SAR) confirmed that the amide group was more beneficial to HDACs inhibition compared with the tertiary amine group.[11] In vitro activity evaluation revealed that **4** showed excellent HDACs inhibition and potent growth inhibition in multiple tumor cell lines. Most importantly, **4** possessed more potent in vivo antitumor activity than its parent compound **1**, and relative to the approved HDACs inhibitor SAHA, **4** exhibited more efficient oral and/or intraperitoneal antitumor activities in a human breast carcinoma (MDA-MB-231) xenograft model, superior oral antimetastatic activity in a mouse hepatoma-22 (H22) pulmonary metastasis model, and comparable oral antitumor activity in a human colon tumor (HCT116) xenograft model.

RESULTS AND DISCUSSION

Chemistry. Compound **4** was prepared following the procedures described in Scheme 1. The tetrahydroisoquinoline ring of **6** was constructed from the starting material 3,5-diiodo-L-tyrosine (**5**) by reaction with formaldehyde under the Pictet−Spengler cyclization conditions. Compound **6** was protected by the Boc group, followed by catalytic hydrogenolysis to give compound **8**. Condensation of **8** with 4-methoxyaniline and subsequent alkylation with bromoacetate gave compound **10**, which was deprotected using trifluoroacetic acid to afford intermediate **11**. The classical peptide synthesis method involving esterification, condensation, and saponification converted L-isoleucine **12** to intermediate **13**, which was installed onto the intermediate **11** to give our target compound **4** after treatment with NH_2OK in methanol.

dx.doi.org/10.1021/jm200577a |*J. Med. Chem.* 2011, 54, 5532–5539

Scheme 1[a]

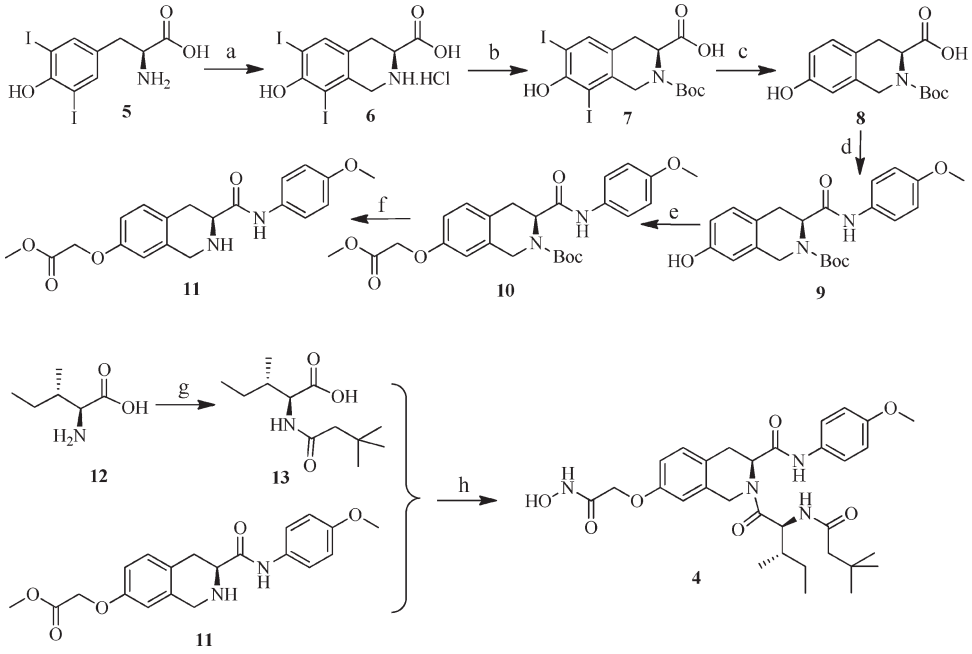

[a] Reagents and conditions: (a) $(CH_2O)_n$, 37%HCl, $CH_3OCH_2CH_2OCH_3$, 72−75 °C, 18 h, 58%; (b) $(Boc)_2O$, 1N NaOH, THF, 95%; (c) 10%Pd−C, H_2, Et_3N, MeOH, 88%; (d) 4-methoxyaniline, CC, HOBT, anhydrous THF, 90%; (e) $BrCH_2COOCH_3$, K_2CO_3, anhydrous DMF, 65%; (f) TFA, CM, saturated Na_2CO_3, 94%; (g) (i) HCl, CH_3OH, (ii) 3,3-dimethylbutanoic acid, isobutyl chloroformate, NMM, THF, (iii) 2M NaOH, C_2H_5OH, 65% for three steps; (h) (i) TBTU, Et_3N, THF, (ii) NH_2OK, CH_3OH, 32% for two steps.

Table 1. HDACs Inhibitory Activity of 4, 1, 2, 3, and SAHA

	IC_{50} (μM)		
compd	HeLa nuclear extract	HDAC6	HDAC8
4	0.052	0.056	0.146
1[a]	0.058	0.047	0.139
2[a]	0.447	0.094	0.263
3[a]	0.297	0.158	0.333
SAHA[a]	0.107	0.195	1.48

[a] Cited from ref 11.

HDACs Inhibition Assay. Compound **4** was evaluated for its in vitro inhibitory activity against HeLa cell nuclear extract (contains primarily HDAC1 and HDAC2), HDAC6 and HDAC8 in order to compare its HDACs inhibitory profile with compounds **1**, **2**, and **3**. Results listed in Table 1 showed that the inhibitory activity of **4** was comparable with that of its parent compound **1** and superior to that of its analogues **2** and **3**, which correlated well with the aforementioned SAR that the oxygen atom of amide group was a significant contributor to HDACs inhibition. Like the other tetrahydroisoquinoline-bearing hydroxamic acid derivatives, compound **4** also did not exhibit any isoform selectivity in our HDACs inhibitory assay.

Antiproliferative Activity Assay. Because of its more potent enzymes inhibitory activity relative to SAHA (Table 1), compound **4** was evaluated for its antiproliferative activity against nine solid or hematological tumor cell lines with SAHA as positive control. Overall, the antiproliferative activity of **4** was considerable with the IC_{50} values against MDA-MB-231, HeLa, HL60, and PC-3 tumor cell lines being lower than those of SAHA (Table 2).

Flow Cytometric Cell Cycle Analysis. Subsequently, the cell cycle profile of the human breast tumor cell line MDA-MB-231 treated with **4** and SAHA was analyzed by flow cytometry. As shown in Figure 3, the action model of **4** on MDA-MB-231 cell cycle is similar to that of SAHA. At low concentrations (0.5 μM for **4**, 1 μM for SAHA), both compounds mainly caused G1 phase arrest, while at high concentrations (2 and 5 μM for **4**, 5 μM for SAHA) an increment of G2 phase population was induced.

In Vivo Antitumor Activity Assay. On the basis of the favorable in vitro activity for **4**, its antitumor activity in the same MDA-MB-231 (human breast tumor) xenograft model as described in our previous research[11] was evaluated. MDA-MB-231 cells (5×10^6) were subcutaneously implanted in the right flanks of female nude mice (BALB/c-nu). When tumor size reached about 100 mm^3, mice were randomized to six per group and were dosed intraperitoneally with our compounds (90 mg/kg/day) or SAHA (90 mg/kg/day) for 19 days. Tumor growth inhibition (TGI) and relative increment ratio (T/C) were calculated at the end of treatment to reveal the antitumor effects in tumor weight and tumor volume, respectively.

$$\mathrm{TGI} = (\text{the mean tumor weight of control group} - \text{the mean tumor weight of treated group}) / \text{the mean tumor weight of control group}$$

Tumor volume (V) was estimated using the equation ($V = ab^2/2$, where a and b stand for the longest and shortest diameter, respectively). T/C was calculated according to the following formula:

$$\frac{T}{C} = \frac{\text{the mean RTV of treated group}}{\text{the mean RTV of control group}}$$

dx.doi.org/10.1021/jm200577a |J. Med. Chem. 2011, 54, 5532–5539

Table 2. Antiproliferative Activities of 4 against Several Tumor Cell Lines with SAHA as Positive Control

	IC_{50} (μM)[a]								
compd	MDA-MB-231	MCF-7	HCT-116	HeLa	K562	NB4	HL60	ES-2	PC-3
4	0.58	3.20	0.77	56.1	3.47	2.69	65.8	12.9	0.83
SAHA	1.31	2.81	0.34	147	3.32	1.52	>200	6.21	1.33

[a] Values are the mean of three experiments. The standard derivations are <20% of the mean.

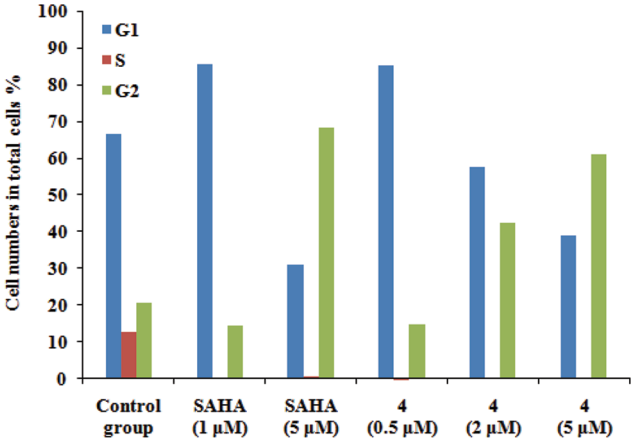

Figure 3. Cell cycle profiles of MDA-MB-231 cells treated with **4** and SAHA at different concentrations.

Table 3. In Vivo Antitumor Activity in the First MDA-MB-231 Xenograft Model[a]

compd	TGI (%)	T/C (%)
SAHA	45	64
1	40	63
2	55	47
3	−9	87
4	79	37

[a] Compared with the control group, all treated groups except compound **3** showed statistically significant ($P < 0.05$) T/C and TGI by Student's two-tailed t test.

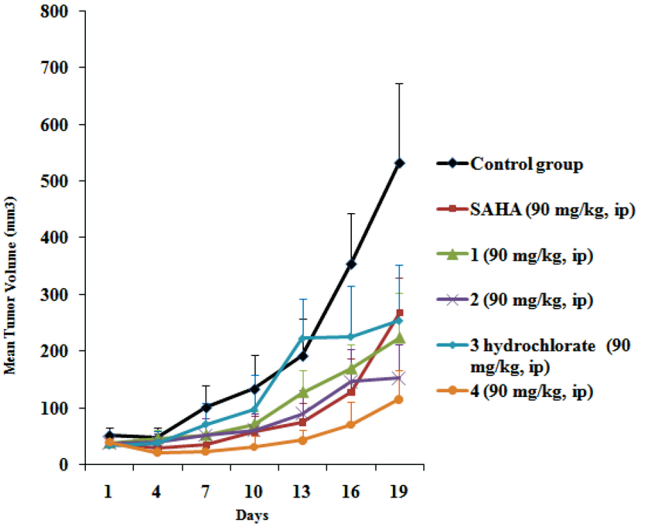

Figure 4. Growth curve of implanted MDA-MB-231 xenograft in nude mice. Data are expressed as the mean ± standard deviation.

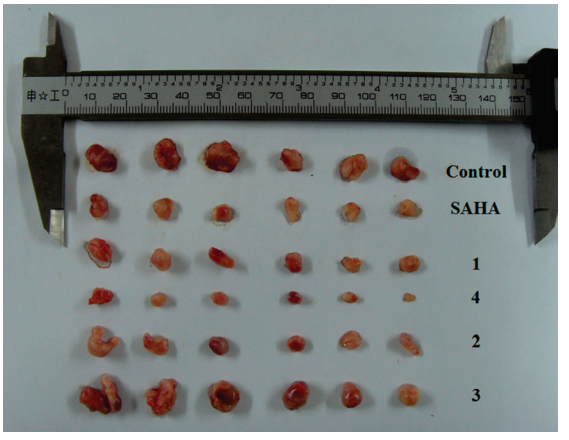

Figure 5. Picture of dissected MDA-MB-231 tumor tissues.

RTV, namely relative tumor volume = V_t/V_0, (V_t: the tumor volume measured at the end of treatment; V_0: the tumor volume measured at the beginning of treatment)

In the MDA-MB-231 xenograft model, compound **4**, with the highest TGI value (79%) and lowest T/C value (37%), demonstrated superior antitumor activity to its parent compound **1**, its analogues **2** and **3**, and the reference compound SAHA after treatment for 19 consecutive days (Table 3). The tumor growth curve depicted in Figure 4 and the final tumor tissue size visualized in Figure 5 also explicitly showed the excellent antitumor potency of **4**.

Considering that compound **4** did not consist of the gastric acid sensitive *tert*-butyl carbamate group compared with its parent compound **1**, another set of experiment in a MDA-MB-231 xenograft model was conducted to check if **4** was oral active. In this experiment, both **4** and SAHA were given by oral administration (po) and intraperitoneal injection (ip). The data showed in Table 4 and Figure 6 validated the results obtained from our first MDA-MB-231 xenograft model that **4** was more potent than SAHA at the same dosing regimen (90 mg/kg/day, ip). The data also indicated that **4** caused tumor growth delay in a dose-dependent manner (The antitumor ability of intraperitoneal 60 mg/kg/day was inferior to that of intraperitoneal 90 mg/kg/day). Notably, at the same dosage (90 mg/kg/day), the oral activity of **4** (TGI = 66%, T/C = 30%) was better than its intraperitoneal activity (TGI = 51%, T/C = 40%), whereas the antitumor activities of SAHA by different administration routes were similar.

On the basis of the above duplicate in vivo experiment results, it was concluded that relative to SAHA, compound **4** exhibited more potent oral and/or intraperitoneal MDA-MB-231 inhibitory activity in a reproducible and dose-dependent manner.

dx.doi.org/10.1021/jm200577a |J. Med. Chem. 2011, 54, 5532–5539

Table 4. In Vivo Antitumor Activity in the Second MDA-MB-231 Xenograft Model[a]

compd	TGI (%)	*T*/*C* (%)
SAHA (90 mg/kg, ip)	43	57
SAHA (90 mg/kg, po)	43	58
4 (90 mg/kg, ip)	51	40
4 (60 mg/kg, ip)	45	62
4 (90 mg/kg, po)	66	30

[a] Compared with the control group, all treated groups showed statistically significant ($P < 0.05$) *T*/*C* and TGI by Student's two-tailed *t* test.

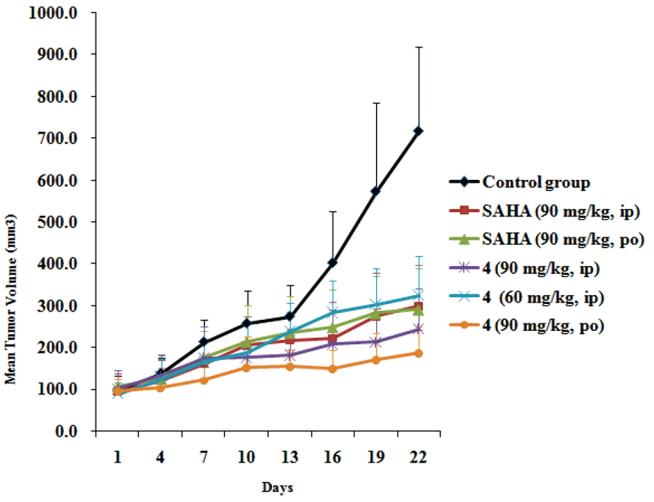

Figure 6. Growth curve of another implanted MDA-MB-231 xenograft in nude mice. Data are expressed as the mean ± standard deviation.

Table 5. In Vivo Antitumor Activity in a HCT116 Xenograft Model[a]

compd	TGI (%)	*T*/*C* (%)
SAHA (90 mg/kg, po)	65	49
4 (60 mg/kg, po)	32	85
4 (90 mg/kg, po)	59	53

[a] Compared with the control group, all treated groups showed statistically significant ($P < 0.05$) *T*/*C* and TGI by Student's two-tailed *t* test.

Encouraged by the potent oral activity of **4** in the MDA-MB-231 xenograft model, we went on to explore its antitumor activity in a HCT116 xenograft model because HCT116 tumor cell line was also sensitive to **4** and SAHA (Table 2). Experiment method was similar to that of the MDA-MB-231 xenograft model. Briefly, HCT116 cells (5×10^6) were subcutaneously implanted in the right flanks of female nude mice (BALB/c-nu). When tumor size reached about 100 mm^3, mice were randomized to six per group. Compound **4** (90 mg/kg/day or 60 mg/kg/day) and SAHA (90 mg/kg/day) were dosed orally by gavage for 19 consecutive days. TGI and *T*/*C* were also used to evaluate the antitumor activity (Table 5). In the HCT116 xenograft model, treatment with **4** and SAHA at the same treated concentration (90 mg/kg/day) yielded similar TGI, 59% versus 65%, and similar *T*/*C*, 53% versus 49%, respectively. Dose-dependent effects of **4** were also concluded from the results shown in Table 5 and Figure 7.

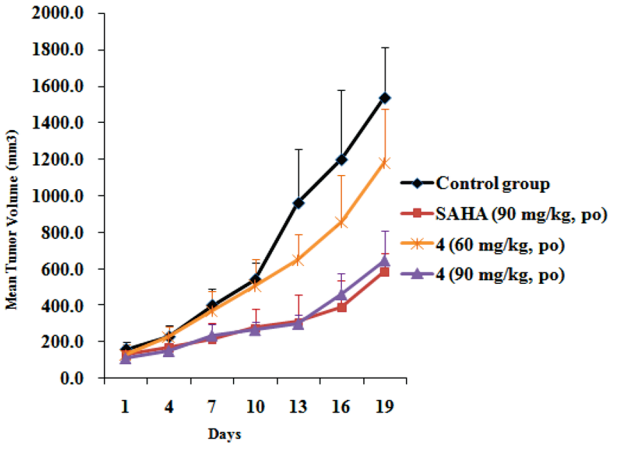

Figure 7. Growth curve of implanted HCT116 xenograft in nude mice. Data are expressed as the mean ± standard deviation.

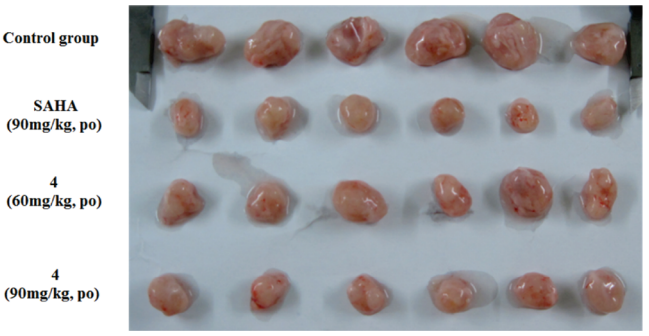

Figure 8. Picture of dissected HCT116 tumor tissues.

And the picture of dissected tumor tissues after treatment is shown in Figure 8. Taken together, in the HCT116 xenograft model, compound **4** exhibited comparable oral antitumor activity with SAHA in a dose-dependent manner.

Given the fact that HDAC6 is involved in tumor cell migration (motility) and angiogenesis,[3] both of which play crucial roles in tumor metastasis processes. Hence, inhibition of HDAC6 should impede tumor metastasis. In fact, it has been reported that HDAC6 selective inhibitor tubacin and MPHA could potently inhibit tumor migration and invasion at the cellular level.[14,15] Recently, the antiangiogenic activities of HDACi in preclinical and clinical studies have been reviewed.[16] On the basis of the promising HDACs inhibitory effects (especially the potent HDAC6 inhibitory activity) of our tetrahydroisoquinoline-bearing hydroxamic acid analogues (Table 1), a mouse pulmonary metastasis model using hepatoma-22 (H22) was established to investigate their in vivo antimetastatic activity. Female Kunming mice were injected via tail vein with approximately 1×10^6 H22 cells suspended in 0.2 mL of saline on the first day. Mice were randomly assigned into seven groups (8 per group) according to the dosing regimen: control group, SAHA (90 mg/kg), **1** (90 mg/kg), **2** (90 mg/kg), **3** (90 mg/kg), **4** (90 mg/kg), and **4** (60 mg/kg). Tested compounds were dosed orally by gavage from the fifth day for 14 consecutive days. After treatment, mice were sacrificed and their lungs were treated with Bouin's solution until macroscopic metastases were infiltrated by white granules with defined borders. The numbers of macroscopic metastatic nodes in the lungs were counted to evaluate the therapeutic

dx.doi.org/10.1021/jm200577a | *J. Med. Chem.* 2011, 54, 5532–5539

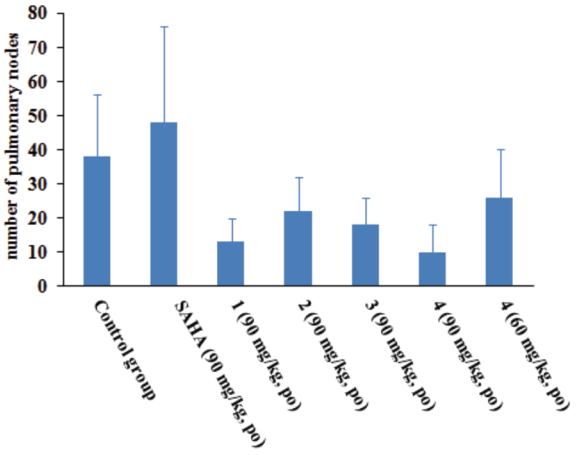

Figure 9. The number of metastatic pulmonary nodes in the mouse hepatoma-22 (H22) pulmonary metastasis model. Data are expressed as the mean ± standard deviation.

effects of tested compounds (Figure 9). The smaller the number of pulmonary metastatic nodes was, the higher potential in reducing metastasis the compound had. Compared with the control group, all the tested compounds, except SAHA, showed statistically significant antimetastatic activity ($P < 0.05$ by Student's two-tailed t test), and compound **4** was the most potent one as it was in the MDA-MB-231 xenograft model.

Unexpectedly, SAHA, the pan-HDACi with effective HDAC6 inhibitory activity, was totally inactive in the metastasis model. This result suggested that our tetrahydroisoquinoline-bearing hydroxamic acid derivatives might target other regulation pathway to influence the tumor metastasis. On the basis of this idea, compounds **1**, **2**, **3**, **4**, and SAHA were evaluated for their inhibitory activity against matrix metalloproteinase 2 (MMP2), another Zn^{2+} dependent metalloprotease involved in tumor invasion and metastasis,[17] and aminopeptidase N (APN/CD13), also a Zn^{2+} dependent metalloprotease responsible for tumor invasion and angiogenesis.[18] MMP2 and APN have been studied as antitumor targets for many years in our lab,[19−24] and several potent APN inhibitors discovered in our lab exhibited effective in vivo antimetastatic activity.[21,22] Preliminary inhibition assay revealed that these tetrahydroisoquinoline-bearing hydroxamic acid derivatives were inactive against MMP2 but exhibited moderate APN inhibitory activity, whereas SAHA was essentially inactive (data not shown), which showed that the inhibitions against HDACs or APN were due to the molecular structures of test compounds rather than the unselective coordination between hydroxamic acid group and zinc ion. Such results also indicated that tetrahydroisoquinoline-bearing hydroxamic acid derivatives might be dual inhibitors of HDACs and APN. The difference in APN inhibition abilities between our target compounds and SAHA could explain their difference in in vivo antimetastatic activity to some extent. Further research should be performed to systematically explore the exact antimetastatic mechanism of our compounds.

In most cases, HDACi appear safe, as induction of mortality and serious adverse effects have not been observed. Frequently occurring dose-limiting toxic effects include reversible fatigue, nausea, vomiting, gastrointestinal disturbances, and transient hematological or myeloid toxicity.[25] On the basis of the currently available data, it is unclear whether such side effects result from certain HDACs isoform inhibition, off-target effects (inhibition of other enzymes), or metabolites of HDACi. In general, isoform-selective HDACi have the potential for less off-target effects, thus less toxicity, meanwhile pan-HDACi are prone to be more toxic due to off-target effects resulting from certain HDACs isoform inhibition. However, pan-HDACi often possess more potent antitumor efficiency because they can block more vital pathways of tumor cells. There is a balance between potency and toxicity, and it remains to be determined whether isoform-selective HDACi will be equally effective but avoid side effects relative to pan-HDACi. As aforementioned, like its analogues **1**, **2**, and **3**, compound **4** also did not exhibit any isoform selectivity in our HDACs inhibitory assay, which indicated that they might be pan-HDACi. In all the above animal experiments, during treatment no significant body weight loss was observed, and after treatment mice were dissected and no signs of evident toxicity were detected in internal organs such as liver and spleen (data not shown). Specific side effects and long-term toxicity of our tetrahydroisoquinoline-bearing hydroxamic acid derivatives need further observation. Preliminary stability assay revealed that compound **4** was stable against artificial gastric juice and artificial intestinal juice (data not shown), which validated our design idea. On the basis of the information that many in vivo active hydroxamic acid derivatives exhibited poor pharmacokinetic parameters (such as low bioavailability, short $t_{1/2}$) in mouse and rat,[26,27] in our research present in this paper, we first evaluated the antitumor potency of our target compounds in in vivo xenograft models instead of examining their pharmacokinetic profiles. As a promising antitumor candidate, detailed and complete pharmacokinetic profiles of compound **4** will be disclosed in our follow-up research.

CONCLUSION

Previously, a novel series of tetrahydroisoquinoline-based hydroxamic acid derivatives were designed and synthesized as HDACs inhibitors. In the present research, further optimization focused on one compound **1**, which was active in vivo. The optimization work led to another oral HDACi **4** with more potent in vivo activity, which was probably due to **4**'s more preferable metabolic stability and oral bioavailability. Related pharmacokinetic research will be carried out in our follow-up study. Compared with the approved HDACi SAHA, **4** exhibited superior in vivo antitumor potency in a MDA-MB-231 xenograft model and similar in vivo antitumor potency in a HCT116 xenograft model. Moreover, in a mouse hepatoma-22 (H22) pulmonary metastasis model, SAHA was totally inactive, whereas **4** possessed high antimetastatic potential, which might result from synergetic aminopeptidase N (APN/CD13) inhibition. Collectively, a potent oral HDACi **4** with dual or even multiple antitumor effects has been discovered. This compound warrants future research and development as a promising antitumor candidate.

EXPERIMENTAL SECTION

Chemistry. All commercially available starting materials, reagents, and solvents were used without further purification unless otherwise stated. All reactions were monitored by TLC with 0.25 mm silica gel plates (60GF-254). UV light, iodine stain, and ferric chloride were used to visualize the spots. Silica gel or C18 silica gel was used for column chromatography purification. ^{1}H NMR spectra were recorded on a Bruker DRX spectrometer at 600 MHz, δ in parts per million and J in hertz, using TMS as an internal standard. High-resolution mass spectra

were conducted by Shandong Analysis and Test Center in Ji'nan, China. ESI-MS spectra were recorded on an API 4000 spectrometer. Melting points were determined uncorrected on an electrothermal melting point apparatus. Compound **4** were >95% pure by HPLC analysis, performed on a Agilent 1100 HPLC instrument using a Phenomenex Synergi 4 μ Polar-RP 80A column (250 mm × 4.6 mm), eluted with 50% acetonitrile/50% water (containing 0.1% formic acid) over 20 min, with detection at 254 nm and a flow rate of 1.0 mL/min.

(*S*)-7-Hydroxy-6,8-diiodo-Tic hydrochloride (**6**), (*S*)-2-(*tert*-butoxycarbonyl)-7-hydroxy-6,8-diiodo-Tic (**7**), (*S*)-2-(*tert*-butoxycarbonyl)-7-hydroxy-Tic (**8**), (*S*)-*tert*-butyl 7-hydroxy-3-((4-methoxyphenyl)carbamoyl)-3,4-dihydroisoquinoline- 2(1*H*)-carboxylate (**9**), and (*S*)-*tert*-butyl 7-(2-methoxy-2-oxoethoxy)-3-((4- methoxyphenyl)carbamoyl)-3,4-dihydroisoquinoline-2(1*H*)-carboxylate (**10**) were synthesized according to the methods in our previous work.[10] (*S*)-Methyl 2-((3-((4-methoxyphenyl)carbamoyl)-1,2,3,4-tetrahydroisoquinolin-7-yl) oxy) acetate (**11**), *tert*-butyl (2*S*,3*S*)-1-((*S*)-7-(2-(hydroxyamino)-2-oxoethoxy)-3-(4-methoxy phenylcarbamoyl)-3,4-dihydroisoquinolin-2(1*H*)-yl)-3-methyl-1-oxopentan-2-ylcarbamate (**1**), *tert*-butyl (2*S*,3*S*)-1-((*S*)-7-(2-(hydroxyamino)-2-oxoethoxy)-3-(4-methoxyphenylcarbamoyl)-3,4-dihydroisoquinolin-2(1*H*)-yl)-3-methylpentan-2-ylcarbamate (**2**), and (*S*)-2-((2*S*,3*S*)-2-(3,3-dimethylbutanamido)-3-methylpentyl)-7-(2-(hydroxyamino)-2-oxoethoxy)-*N*-(4-methoxyphenyl)-1,2,3,4-tetrahydroisoquinoline-3-carboxamide (**3**) were obtained as described previously.[11]

(2*S*,3*S*)-2-(3,3-Dimethylbutanamido)-3-methylpentanoic Acid (13). According to the similar procedures described by our group,[28] L-isoleucine **12** was converted to **13** as colorless crystal; mp 143−145 °C. ^{1}H NMR (DMSO-d_6) δ 0.83−0.86 (m, 6H), 0.95 (s, 9H), 1.16−1.22 (m, 1H), 1.38−1.44 (m, 1H), 1.72−1.78 (m, 1H), 2.03 (d, J = 12.6 Hz, 1H), 2.07 (d, J = 12.6 Hz, 1H), 4.15 (dd, J = 8.4 Hz, J = 6.6 Hz, 1H), 7.83 (d, J = 8.4 Hz, 1H), 12.46 (s, 1H). ESI-MS m/z: 230.2 $[M + H]^+$.

(*S*)-2-((2*S*,3*S*)-2-(3,3-Dimethylbutanamido)-3-methylpentanoyl)-7-(2-(hydroxyamino)-2-oxoethoxy)-*N*-(4-methoxyphenyl)-1,2,3,4-tetrahydroisoquinoline-3-carboxamide (4). At room temperature, to a solution of compound **13** (1.15 g, 5.0 mmol) in anhydrous THF (30 mL), was added Et_3N (0.56 g, 5.5 mmol) followed by 2-(1*H*-benzotriazole-1-yl)-1,1,3,3-tetramethyluronium tetrafluoroborate (TBTU, 1.78 g, 5.5 mmol). After 15 min, the amine compound **11** (1.85 g, 5.0 mmol) was added. Stirring was continued overnight, and then THF was evaporated with the residue being taken up in EtOAc (40 mL). The EtOAc solution was washed with saturated Na_2CO_3 (3 × 10 mL), 1 N HCl (3 × 10 mL), and brine (3 × 10 mL), dried over $MgSO_4$, and evaporated under vacuum. The obtained crude product was treated with a solution of NH_2OK in anhydrous methanol for 1 h, and then the solvent was evaporated under vacuum. The residue was acidified with 2 N HCl until pH 5−6 and then extracted with EtOAc (3 × 30 mL). The organic layers were combined, washed with brine (3 × 20 mL), dried over $MgSO_4$, and evaporated, with the residue being purified by C18 reversed-phase column chromatography (H_2O/MeOH 3:7) to give desired compound **4** (0.93 g, 32% yield) as a white powder; mp 123−125 °C. ^{1}H NMR (DMSO-d_6) δ 0.87 (t, J = 7.2 Hz, 3H), 0.92 (d, J = 6.0 Hz, 3H), 0.97 (s, 9H), 1.09−1.15 (m, 1H), 1.33−1.37 (m, 1H), 1.73−1.76 (m, 1H), 2.03 (d, J = 12.6 Hz, 1H), 2.18 (d, J = 12.6 Hz, 1H), 2.95−2.99 (m, 1H), 3.21−3.26 (m, 1H), 3.69 (s, 3H), 4.42 (s, 2H), 4.83 (d, J = 15.6 Hz, 1H), 4.90 (d, J = 15.6 Hz, 1H), 4.64−4.67 (m, 1H), 5.14−5.16 (m, 1H), 6.73−6.89 (m, 4H), 7.08−7.09 (m, 1H), 7.50−7.52 (m, 2H), 8.14 (d, J = 8.4 Hz, 1H), 8.98 (s, 1H), 9.35 (s, 1H), 10.83 (s, 1H). HRMS (AP-ESI) m/z calcd for $C_{31}H_{43}N_4O_7$ $[M + H]^+$ 583.3132, found 583.3165. Retention time: 6.5 min.

In Vitro HDACs Inhibition Fluorescence Assay. In vitro HDACs inhibition assays were conducted as previously described.[11] In brief, 10 μL of enzyme solution (HeLa nuclear extract, HDAC6, or HDAC8) was mixed with various concentrations of tested compound (50 μL). Five minutes later, fluorogenic substrate Boc-Lys (acetyl)-AMC (40 μL) was added, and the mixture was incubated at 37 °C for 30 min and then stopped by addition of 100 μL of developer containing trypsin and TSA. After incubation at 37 °C for 20 min, fluorescence intensity was measured using a microplate reader at excitation and emission wavelengths of 390 and 460 nm, respectively. The inhibition ratios were calculated from the fluorescence intensity readings of tested wells relative to those of control wells, and the IC_{50} values were calculated using a regression analysis of the concentration/inhibition data.

In Vitro Antiproliferative Assay. In vitro antiproliferative assays were determined by the MTT (3-[4,5-dimethyl-2-thiazolyl]-2,5-diphenyl-2*H*-tetrazolium bromide) method as previously described.[11] Briefly, all cell lines were maintained in RPMI1640 medium containing 10% FBS at 37 °C in 5% CO_2 humidified incubator. Cells were passaged the day before dosing into a 96-well cell plate and allowed to grow for a minimum of 4 h prior to addition of compounds. After compounds addition, the plates were incubated for an additional 48 h, and then 0.5% MTT solution was added to each well. After further incubation for 4 h, formazan formed from MTT was extracted by adding 200 μL of DMSO for 15 min. Absorbance was then determined using an ELISA reader at 570 nm, and the IC_{50} values were calculated according to the inhibition ratios.

In Vitro Cell Cycle Analysis. MDA-MB-231 cells were seeded into six-well plates at a density of 4 × 10^5 per well. After overnight incubation, cells were treated with **4** and SAHA. After 48 h treatment, cells were harvested and fixed with 70% ethanol phosphate buffer overnight. Then the cells were washed with PBS twice, incubated with DNase-free RNase A (1 mg/mL, Solarbio, China) for 30 min, and stained with propidium iodide (50 mg/mL, Solarbio, China) for 30 min, avoiding light at room temperature. DNA content was measured by a fluorescence-activated cell cytometer (FACScan, Becton Dickinson, USA) and analyzed by MODFit LT for Mac V3.0 software.

In Vivo Human Tumor Xenograft Models. In vivo human tumor xenograft models were established as previously described.[11] In brief, tumor cell lines (MDA-MB-231 and HCT116) were cultured in RPMI1640 medium containing 10% FBS and maintained in a 5% CO_2 humidified incubator at 37 °C. For in vivo antitumor assays, aforementioned cells were inoculated subcutaneously in the right flanks of female athymic nude mice (BALB/c-nu, 5−6 weeks old, Slac Laboratory Aniamal, Shanghai, China). About 10 days after injection, tumors were palpable (about 100 mm^3) and mice were randomized into treatment and control groups (6 mice per group). The treatment groups received specified concentrations of compounds by oral administration or intraperitoneal injection, and the blank control group received an equal volume of PBS solution containing DMSO. During treatment, subcutaneous tumors were measured with a vernier caliper every three days, and body weight was monitored regularly. After treatment, mice were sacrificed and dissected to weigh the tumor tissues and to examine the internal organ injury. All the obtained data were used to evaluate the antitumor potency and toxicity of compounds. Data were analyzed by Student's two-tailed t test. A P level <0.05 was considered statistically significant.

In Vivo Mouse H22 Pulmonary Metastasis Model. The mouse hepatoma H22 cell line used in this study was a kind gift form Professor Cui (Shandong Academy of Medical Sciences, China). Female Kunming mice were purchased from Center for New Drugs Evaluation of Shandong University, China. For in vivo antimetastasis assays, H22 cells suspended in saline were injected into female Kunming mice (7−8 weeks old) via tail vein on the first day. Mice were randomly assigned into treatment and control groups (eight mice per group). After 4 days, tested compounds were dosed orally by gavage. During treatment, body weight was monitored regularly. After treatment, mice were sacrificed to examine the abdomen and chest. The metastatic nodes in lungs were visualized by Bouin's solution and counted to evaluate the therapeutic effects of tested compounds.

■ ASSOCIATED CONTENT

Supporting Information. ^{1}H NMR spectral information of the key intermediate **13** and the target compound **4**. HPLC analysis chromatogram of the target compound **4**. This material is available free of charge via the Internet at http://pubs.acs.org.

■ AUTHOR INFORMATION

Corresponding Author
*Phone: 86-531-88382264. Fax: 86-531-88382264. E-mail: wfxu@yahoo.cn.

■ ACKNOWLEDGMENT

This work was supported by National Nature Science Foundation of China (grant no. 30772654 and no. 36072541), National High Technology Research and Development Program of China (863 project; grant no. 2007AA02Z314), National Science and Technology Major Project (grant no. 2009ZX09103-118), and Academic Award for Young Doctoral Postgraduate of Ministry of Education of China

■ ABBREVIATIONS USED

HDAC, histone deacetylase; HDACi, histone deacetylase inhibitor; SAR, structure−activity relationship; SAHA, suberoylanilide hydroxamic acid; ZBG, zinc-binding group; Boc, tertiary butoxycarbonyl; TGI, tumor growth inhibition; *T*/*C*, relative increment ratio

■ REFERENCES

(1) Wolffe, A. P. Histone deacetylase: a regulator of transcription. *Science* **1996**, *272*, 371–372.
(2) Glozak, M. A.; Sengupta, N.; Zhang, X.; Seto, E. Acetylation and deacetylation of non-histone proteins. *Gene* **2005**, *363*, 15–23.
(3) Witt, O.; Deubzer, H. E.; Milde, T.; Oehme, I. HDAC family: What are the cancer relevant targets? *Cancer Lett.* **2009**, *277*, 8–21.
(4) Miller, T. A.; Witter, D. J.; Belvedere, S. Histone deacetylase inhibitors. *J. Med. Chem.* **2003**, *46*, 5097–5116.
(5) Paris, M.; Porcelloni, M.; Binaschi, M.; Fattori, D. Histone deacetylase inhibitors: from bench to clinic. *J. Med. Chem.* **2008**, *21*, 1505–1529.
(6) Grant, S.; Easley, C.; Kirkpatrick, P. Vorinostat. *Nature Rev. Drug Discovery* **2007**, *6*, 21–22.
(7) Campas-Moya, C. Romidepsin for the treatment of cutaneous T-cell lymphoma. *Drugs Today* **2009**, *45*, 787–795.
(8) de Ruijter, A. J.; van Gennip, A. H.; Caron, H. N.; Kemp, S.; van Kuilenburg, A. B. Histone deacetylases (HDACs): characterisation of the classical HDAC family. *Biochem. J.* **2003**, *370*, 737–749.
(9) Vaquero, A. The conserved role of sirtuins in chromatin regulation. *Int. J. Dev. Biol.* **2009**, *53*, 303–322.
(10) Zhang, Y.; Feng, J.; Liu, C.; Zhang, L.; Jiao, J.; Fang, H.; Su, L.; Zhang, X.; Zhang, J.; Li, M.; Wang, B.; Xu, W. Design, synthesis and preliminary activity assay of 1,2,3,4-tetrahydroisoquinoline-3-carboxylic acid derivatives as novel histone deacetylases (HDACs) inhibitors. *Bioorg. Med. Chem.* **2010**, *18*, 1761–1772.
(11) Zhang, Y.; Feng, J.; Jia, Y.; Wang, X.; Zhang, L.; Liu, C.; Fang, H.; Xu, W. Development of tetrahydroisoquinoline-based hydroxamic acid serivatives: potent histone deacetylase inhibitors with marked in vitro and in vivo antitumor activities. *J. Med. Chem.* **2011**, *54*, 2823–2838.
(12) Wilson, I. B.; Harrison, S.; Ginsburg, S. Carbamyl derivatives of acetylcholinesterase. *J. Biol. Chem.* **1961**, *236*, 1498–1500.
(13) O'Brien, R. D.; Hilton, B. D.; Gilmour, L. The reaction of carbamates with cholinesterase. *Mol. Pharmacol.* **1966**, *2*, 593–605.
(14) Tran, A. D.; Marmo, T. P.; Salam, A. A.; Che, S.; Finkelstein, E.; Kabarriti, R.; Xenias, H. S.; Mazitschek, R.; Hubbert, C.; Kawaguchi, Y.; Sheetz, M. P.; Yao, T. P.; Bulinski, J. C. HDAC6 deacetylation of tubulin modulates dynamics of cellular adhesion. *J. Cell Sci.* **2007**, *120*, 1469–1479.
(15) Batovska, D. I.; Kim, D. H.; Mitsuhashi, S.; Cho, Y. S.; Kwon, H. J.; Ubukata, M. Hydroxamic acid derivatives of mycophenolic acid inhibit histone deacetylase at the cellular level. *Biosci., Biotechnol., Biochem.* **2008**, *72*, 2623–2631.
(16) Ellis, L.; Hammers, H.; Pili, R. Targeting tumor angiogenesis with histone deacetylase inhibitors. *Cancer Lett.* **2009**, *280*, 145–153.
(17) Björklund, M.; Koivunen, E. Gelatinase-mediated migration and invasion of cancer cells. *Biochim. Biophys. Acta* **2005**, *1755*, 37–69.
(18) Bauvois, B.; Dauzonne, D. Aminopeptidase-N/CD13 (EC 3.4.11.2) Inhibitors: Chemistry, Biological Evaluations, and Therapeutic Prospects. *Med. Res. Rev.* **2006**, *26*, 88–130.
(19) Cheng, X.; Wang, Q.; Fang, H.; Tang, W.; Xu, W. Synthesis of new sulfonyl pyrrolidine derivatives as matrix metalloproteinase inhibitors. *Bioorg. Med. Chem.* **2008**, *16*, 7932–7938.
(20) Cheng, X.; Wang, Q.; Fang, H.; Tang, W.; Xu, W. Design, synthesis and preliminary evaluation of novel pyrrolidine derivatives as matrix metalloproteinase inhibitors. *Eur. J. Med. Chem.* **2008**, *43*, 2130–2139.
(21) Li, Q.; Fang, H.; Wang, X.; Hu, L.; Xu, W. Novel cyclic-imide peptidomimetics as aminopeptidase N inhibitors. Design, chemistry and activity evaluation. Part I. *Eur. J. Med. Chem.* **2009**, *44*, 4819–4825.
(22) Li, Q.; Fang, H.; Wang, X.; Xu, W. Novel cyclic-imide peptidomimetics as aminopeptidase N inhibitors. Structure-based design, chemistry and activity evaluation. II. *Eur. J. Med. Chem.* **2010**, *45*, 1618–1626.
(23) Wang, Q.; Chen, M.; Zhu, H.; Zhang, J.; Fang, H.; Wang, B.; Xu, W. Design, synthesis, and QSAR studies of novel lysine derives as amino-peptidase N/CD13 inhibitors. *Bioorg. Med. Chem.* **2008**, *16*, 5473–5481.
(24) Su, L.; Fang, H.; Yang, K.; Xu, Y.; Xu, W. Design, synthesis and biological evaluation of novel L-lysine ureido derivatives as aminopeptidase N inhibitors. *Bioorg. Med. Chem.* **2011**, *19*, 900–906.
(25) Elaut, G.; Rogiers, V.; Vanhaecke, T. The Pharmaceutical Potential of Histone Deacetylase Inhibitors. *Curr. Pharm. Des.* **2007**, *13*, 2584–2620.
(26) Thaler, F.; Colombo, A.; Mai, A.; Amici, R.; Bigogno, C.; Boggio, R.; Cappa, A.; Carrara, S.; Cataudella, T.; Fusar, F.; Gianti, E.; di Ventimiglia, S. J.; Moroni, M.; Munari, D.; Pain, G.; Regalia, N.; Sartori, L.; Vultaggio, S.; Dondio, G.; Gagliardi, S.; Minucci, S.; Mercurio, C.; Varasi, M. Synthesis and biological evaluation of *N*-hydroxyphenylacrylamides and *N*-hydroxypyridin-2-ylacrylamides as novel histone deacetylase inhibitors. *J. Med. Chem.* **2010**, *53*, 822–839.
(27) Wang, H.; Yu, N.; Chen, D.; Lee, K. C.; Lye, P. L.; Chang, J. W.; Deng, W.; Ng, M. C.; Lu, T.; Khoo, M. L.; Poulsen, A.; Sangthongpitag, K.; Wu, X.; Hu, C.; Goh, K. C.; Wang, X.; Fang, L.; Goh, K. L.; Khng, H. H.; Goh, S, K.; Yeo, P.; Liu, X.; Bonday, Z.; Wood, J. M.; Dymock, B. W.; Kantharaj, E.; Sun, E. T. Discovery of (2*E*)-3-{2-Butyl-1-[2-(diethylamino)ethyl]-1*H*-benzimidazol-5-yl}-*N*-hydroxyacrylamide (SB939), an Orally Active Histone Deacetylase Inhibitor with a Superior Preclinical Profile. *J. Med. Chem.*, **2011**, DOI: 10.1021/jm2003552.
(28) Mou, J.; Fang, H.; Liu, Y.; Shang, L.; Wang, Q.; Zhang, L.; Xu, W. Design, synthesis and premary activity assay of bi- or tri- peptide analogues with the scaffold L-arginine as amino-peptidase N/CD13 inhibitors. *Bioorg. Med. Chem.* **2010**, *18*, 887–895.